Exhaust Plume Characteristics of Quasi-Steady MPD Thrusters

Hirokazu Tahara, Yoichi Kagaya and Takao Yoshikawa
Division of Mechanical Science, Dept. of Systems and Human Science
Graduate School of Engineering Science, Osaka University
1-3, Machikaneyama, Toyonaka, Osaka 560-8531, Japan
+81-6-6850-6178
tahara@me.es.osaka-u.ac.jp

IEPC-01-133

The quasi-steady MPD thruster MY-III was operated to study the exhaust plasma plume characteristics. Both emission spectroscopic and rotatable double probe measurements were made to evaluate electron temperatures, plasma number densities and plasma flow directions. Flowfield calculation was also carried out to understand plasma flow features and acceleration processes. The plasma was slightly expanded radially outward downstream within the extrapolation line of the divergent nozzle regardless of discharge current and gas species although it was intensively expanded outside the line. Both the electron temperature and the plasma number density decreased radially outward at a constant axial position. The angle of radial expansion for H_2 was relatively small compared with cases for Ar because of an intensive thermal pinch effect for H_2. The calculated physical properties qualitatively agreed with the measured ones even with a simple calculation model. The calculated ion flux gradually decreased downstream, and a large fraction of 90 % of ion flux existed within a radius nearly along the nozzle extrapolation line.

Introduction

The magnetoplasmadynamic (MPD) arcjet is a promising thruster for exploration to deep space and for raising orbits of large space structures. The MPD arcjet utilizes principally electromagnetic force, i.e., Lorentz force, which is generated by electromagnetic interaction between discharge current and magnetic field azimuthally induced by the discharge current. The thrust depends only on the discharge current and does not basically on propellant species because of electromagnetic acceleration. However, in an MPD discharge chamber, complicated chemical reactions involving dissociation and ionization are expected to occur together with the acceleration processes[1]-[4]. Consequently, it has been recognized that the performance characteristics on the discharge voltage, thrust efficiency and electrode erosion depend on propellant species and electrode geometry.

Recently, several kinds of electric thrusters are under use in space and practically under development. It is important to understand exhaust plasma plume characteristics and to estimate interactions between spacecraft and them. In MPD thruster R&D, because the complicated plasma structure is created inside the discharge chamber, it is expected to strongly influence the exhaust plume feature. However, the downstream plasma and flowfield characteristics are not clear.

The quasi-steady MPD thruster MY-III is operated to study the exhaust plume characteristics. Both emission spectroscopic and rotatable double probe measurements are made to evaluate electron temperatures, plasma number densities and plasma flow directions in the downstream plume region. Flowfield calculation is also carried out to understand plasma flow features and acceleration processes in detail. The calculated results are compared with the experimental ones.

Experimental Apparatus

Figure 1 shows a cross sectional view of the quasisteady MPD arcjet used for this study. The arcjet, which is called the MY-III arcjet, is provided with a straight-diverging anode made of copper. The anode nozzle is 58 mm in exit diameter and has a 20-deg half-angle. A cylindrical cathode 17.5 mm in length and 9.5 mm in diameter is made of thoriated tungsten.

Propellants are injected with a cathode slit/anode slit ratio of 50/50 into the discharge chamber through a fast acting valve

* Presented as Paper IEPC-01-133 at the 27th International Electric Propulsion Conference, Pasadena, CA, 15-19 October,2001.

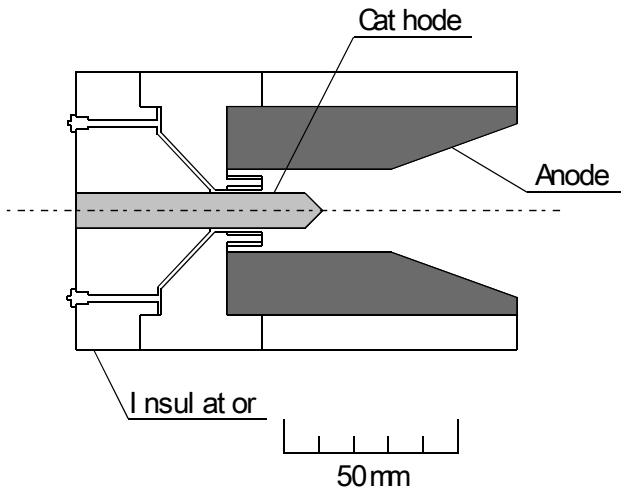

Figure 1 Cross sectional view of quasi-steady MPD arcjet thruster MY-III.

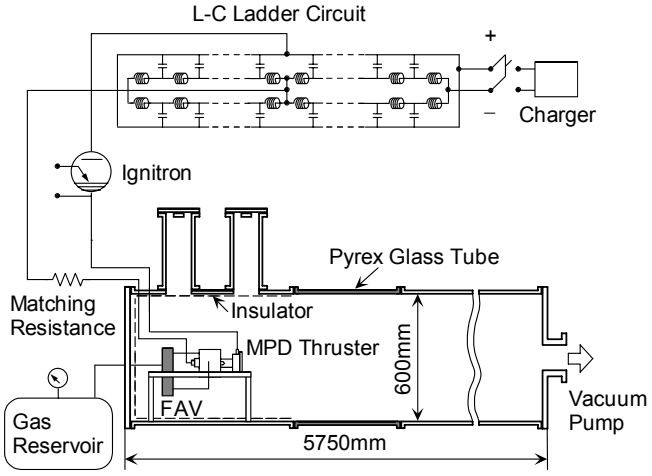

Figure 2 Experimental system with pulse forming network, fast acting valve and MPD thruster.

(FAV) fed from a high pressure reservoir. The rise time and width of the gas pulse, measured with a fast ionization gauge, are 0.5 and 6 msec, respectively. Hydrogen and argon are used as the propellant. The mass flow rates are controlled by adjustment of the reservoir pressure and the orifice diameter of the FAV.

As shown in Fig.2, the main power-supplying pulse forming network, which is capable of storing 62 kJ at 8 kV, delivers a single nonreversing quasisteady current of a maximum of 27 kA with a pulse width of 0.6 msec. A vacuum tank 5.75 m in length and 0.6 m in diameter, where the arcjet is fired, is evacuated to some 10^{-3} Pa prior to each discharge.

Discharge currents are measured by a Rogowski coil calibrated with a known shunt resistance. Voltage

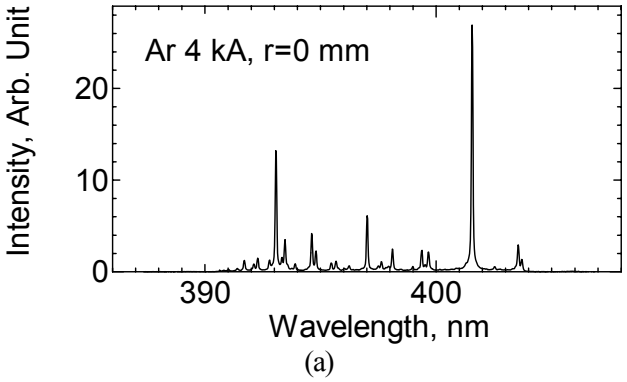

(a)

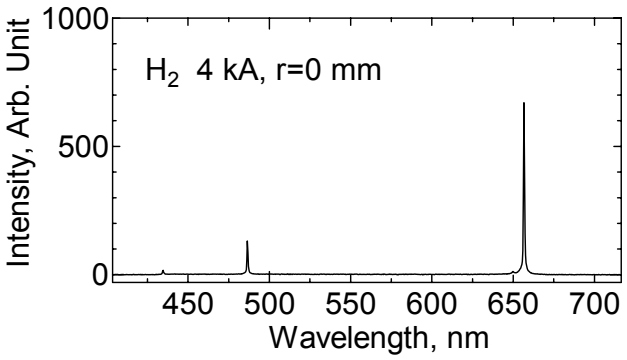

(b)

Figure 3 Typical spectra emitted from MPD plasma at nozzle exit. (a) Ar, 1.37 g/s, 4 kA; (b) H_2, 0.40 g/s, 8 kA.

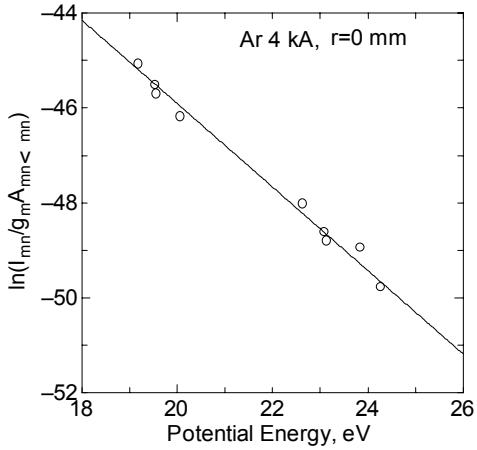

Figure 4 Typical Boltzmann plotting for determination of electronic excitation temperature with ArII lines at Ar, 1.37 g/s and 4 kA.

measurement is performed with a current probe (Iwatsu CP-502), which detects the small current bled through a known resistor (10 k Ω) between the electrodes.

Emission spectroscopic measurement is conducted as

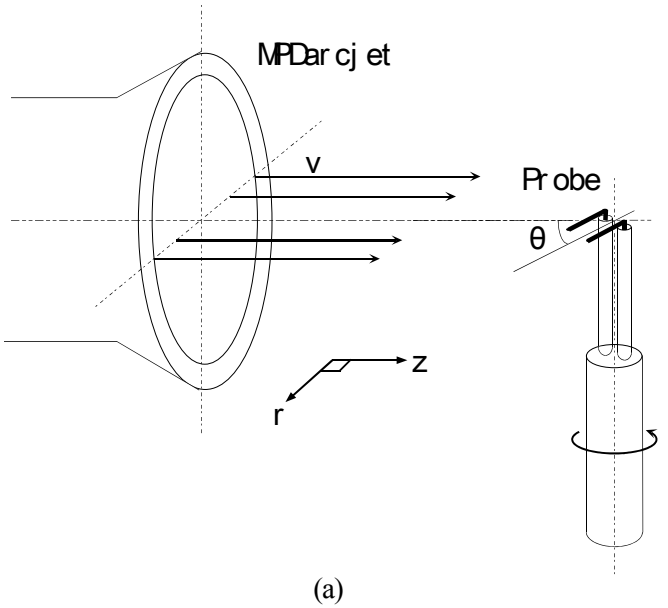

(a)

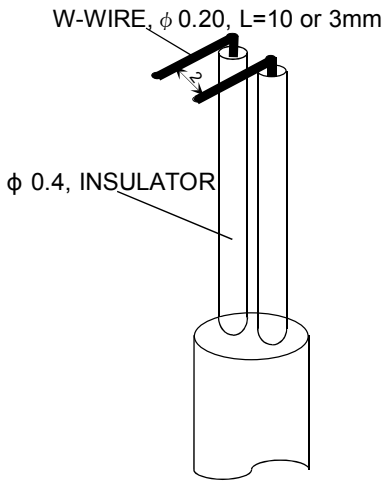

(b)

Figure 5 Rotatable electrostatic double probe system for measurement of plasma flow direction, electron temperature and plasma number density. (a) probe and plasma flow arrangement; (b) probe structure.

reliable plasma disgnostic ones both inside and outside the discharge chamber. Light comes from MPD plasma. Then, the emission is collected by a lens of 80 mm in focal length and is introduced into a 0.5 m monochrometer through an optical fiber. The monochrometer of diffraction-grating-type HAMAMATSU C5095 is provided with a 2400 grooves/mm grating plate and a 1024-channel diode array detector, achieving a spectral resolution of 0.05 nm per detector channel. The measurement is conducted in a steady-state condition by avoiding transitional phenomena near the start of the discharge. The emission is measured for a period of 0.4 msec after 0.2 msec from the discharge

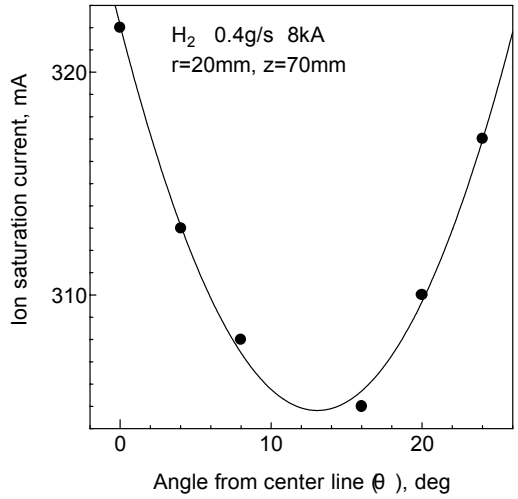

Figure 6 Typical characteristics of ion saturation current of rotatable double probe dependent on angle of probe line to plasma flow.

ignition. The timing is controlled with a gate of the image intensifier, which can open or close the entrance to the array detector.

Electron number densities and electronic excitation temperatures are determined using the spectral data. Because the electronic excitation temperature is almost equal to the free electron temperature in MPD plasma conditions, the former is called electron temperature in this paper. The electron number density is estimated from the stark width of the hydrogen H_β line 486.1 nm. For Ar gas, a small amount of H_2 is added. The spectral intensities measured in this experiment are line-of-sight values, measured by looking through the arc from the side perpendicular to the central line of the arcjet. For line-of-sight measurements, the intensity values correspond to the integrated values of intensity as a function of position. The radially dependent emission coefficient is determined from the measured intensities using well-known Abel transformations. The horizontally average spectral intensities are measured with a vertical interval of 1.0 mm. As shown in Figs.3 and 4, the Ar^+-ion electronic excitation temperature is determined with several ArII lines using a relative intensity method of spectral lines, i.e., by means of Boltzmann plotting, under the assumption of local thermodynamical equilibrium. The H-atom electronic excitation temperature is also determined with HI Balmer lines of 434.0, 486.1 and 656.3 nm.

Electrostatic double probe measurement is carried out to examine exhaust plasma plume features. Electron temperatures and ion (electron) number densities are evaluated. Furthermore, as shown in Fig.5, plasma flow directions are inferred with a rotatable cylindrical probe. When rotating the probe, the ion saturation current, as shown in Fig.6, has a minimum at the special condition that the

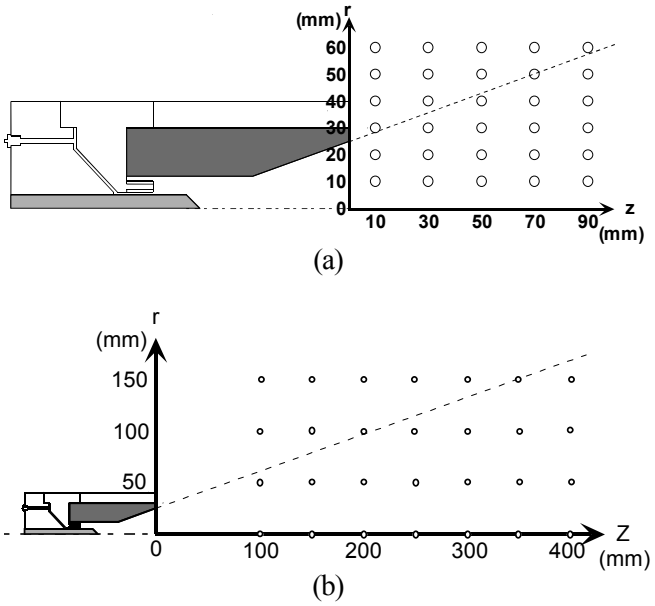

Figure 7 Measurement points for rotatable double probe. (a) near divergent nozzle exit; (b) downstream region.

plasma flows parallel to the probe axis. We can determine a flow direction from the angle. As shown in Fig.7, measurements are conducted in a large region downstream from the arcjet nozzle exit.

Flowfield Calculation

Axisymmetric MPD flowfield is numerically calculated to simply predict argon plasma plume characteristics[3],[5]. In this calculation, we assume that (1) velocities of electron, ion and neutral are equal, i.e., one-fluid model; (2) electron temperature equals heavy species temperature, i.e., one temperature model; (3) nonequilibrium first-ionization and recombination processes are considered; (4) the Hall effect and viscosity are neglected, and (5) heat conduction is considered. Conservation equations of mass, momentum and energy in addition to the magnetic field equation are a group of modified Euler equations.

The Total Variation Diminishing (TVD)-MacCormack scheme with Roe-Yee-Davis's dissipation term is used[6]. In addition, a point-implicit method is also included in order to stabilize numerical oscillation due to ionization and recombination terms, which are sensitive to temperature. The induction equation of magnetic field is solved by the successive over relaxation method, and time-dependent term is removed because we want to get only a steady-state solution. A steady-state solution is obtained by solving both the Euler equations and the magnetic field equation alternatively with coupling them together.

At the gas inlet, i.e., at the upstream end of the discharge chamber, the discharge current, the mass flow rate, the degree of ionization and the temperature are fixed to 4 kA, 1.37 g/s, 0.001 and 5000 K, respectively. The gas is injected with a subsonic velocity. Slip condition is adapted on the electrodes.

Results and Discussion

Electron Temperature and Plasma Number Density at Nozzle Exit

Figures 8 and 9 show the radial distributions of electron temperature and plasma number density, respectively, on the arcjet nozzle exit with Ar and H_2. They are estimated from spectroscopic measurement. Both the electron temperature and the plasma number density have peaks at the central axis and decrease radially outward with a constant discharge current regardless of gas species.

As shown in Fig.8, the electron temperature increases with discharge current at a constant radial position, and particularly at the highest discharge current of 12 kA the electron temperature reaches above 20000 K at the center. However, it decreases to about 15000 K for Ar and about 8000 K for H_2 at a radial position of 25 mm regardless of discharge current; that is, the electron temperature intensively decreases radially outward at 12 kA although it gradually decreases at 4 kA for Ar and at 4 and 8 kA for H_2.

In the plasma number density characteristics, as shown in Fig.9, the Ar plasma densities at 8 and 12 kA are higher than that at 4 kA at a constant radial position although they decrease to about 3.9×10^{20} m^{-3} at 25 mm regardless of discharge current. The profile at 8 kA is almost the same one at 12 kA. In other words, the plasma density intensively decreases radially outward at 8 and 12 kA although it gradually decreases at 4 kA. For H_2, the plasma density at 8 kA is higher than that at 12 kA at a constant radial position, and at 4 kA it is the lowest. The profile at 8 kA is a flat-like one near the central axis. This is expected because the plasma at 12 kA is intensively pinched, thermally and electromagnetically, radially inward near the central axis, i.e., in the cathode jet, compared with the case at 8 kA. In other words, a radially broad plasma is created at 8 kA.

Electron Temperature, Plasma Number Density and Plasma Flow Direction in Exhaust Plume

Figures10 and 11 show the plasma flow patterns in the exhaust plumes from the nozzle exit to an axial position of 90 mm and from 100 to 400 mm, respectively. Only the direction of arrows is important, and the length is arbitrary ones. The dashed lines represent the extrapolation line of the divergent nozzle. The plasma is slightly expanded radially outward downstream within the dashed line, i.e., the nozzle extrapolation line, regardless of gas species; then, near the central axis, i.e., in the cathode jet, it almost flows

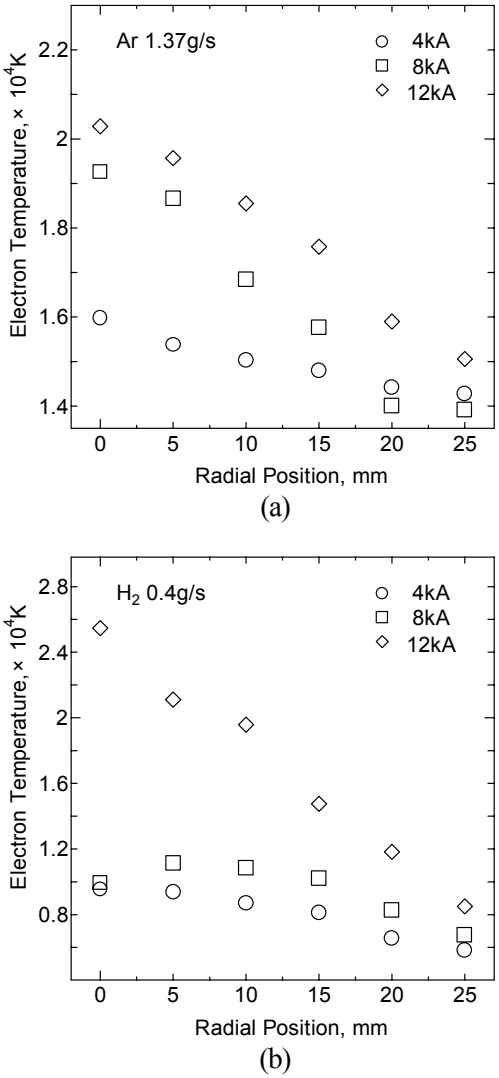

Figure 8 Radial distributions of electron temperature on arcjet nozzle exit with Ar and H_2 by emission spectroscopic measurement. (a) Ar, 1.37 g/s; (b) H_2, 0.40 g/s.

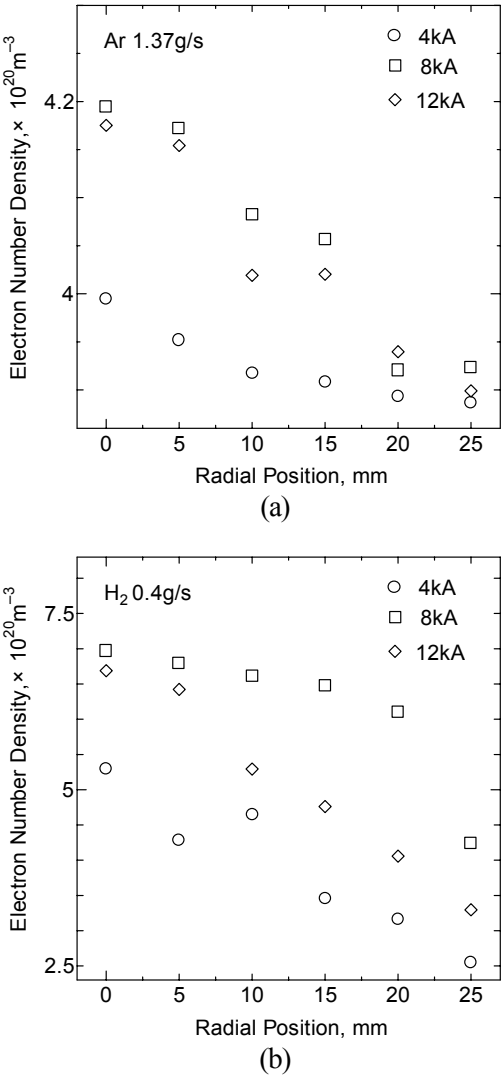

Figure 9 Radial distributions of plasma number density on arcjet nozzle exit with Ar and H_2 by emission spectroscopic measurement. (a) Ar, 1.37 g/s; (b) H_2, 0.40 g/s.

parallel to the axis, although it is intensively expanded outside the line. In other words, the angle of radial expansion is below the half angle of the nozzle, 20 deg, within the dashed line although it is above the half angle outside the dashed line. Therefore, the plasma flow is divided into inner and outer flows with the nozzle extrapolation line.

As shown in Figs.10(a), 10(b), 11(a) and 11(b), the radial expansion of the Ar plasma at 4 kA is relatively large compared with that at 8 kA. This is expected because the plasma is with a higher axial velocity at a larger discharge current. When comparing the pattern at 8 kA for H_2 with that for Ar, as shown in Figs.10(b), 10(c), 11(b) and 11(c), the angle of radial expansion for H_2 is relatively small because of an intensive thermal pinch effect for H_2.

Figures 12 and 13 show the axial distributions of electron temperature and plasma number density, respectively, in the exhaust plumes. They are estimated from probe measurement. Both the electron temperature and the plasma number density decrease radially outward at a constant axial position. They decrease downstream at radial positions of 0 and 50 mm, i.e., within a radial position of 50 mm, although they have peaks at 100 and 150 mm regardless of gas species. The peaks are located near the boundary between the inner and outer flows, i.e., near the extrapolation line of the divergent nozzle. Therefore, it is inferred that an intensive radial expansion occurs in the outer flow and that the electron temperature and the plasma density are seen to decrease axially. In the inner flow, a large amount of thermal energy is expected to be smoothly

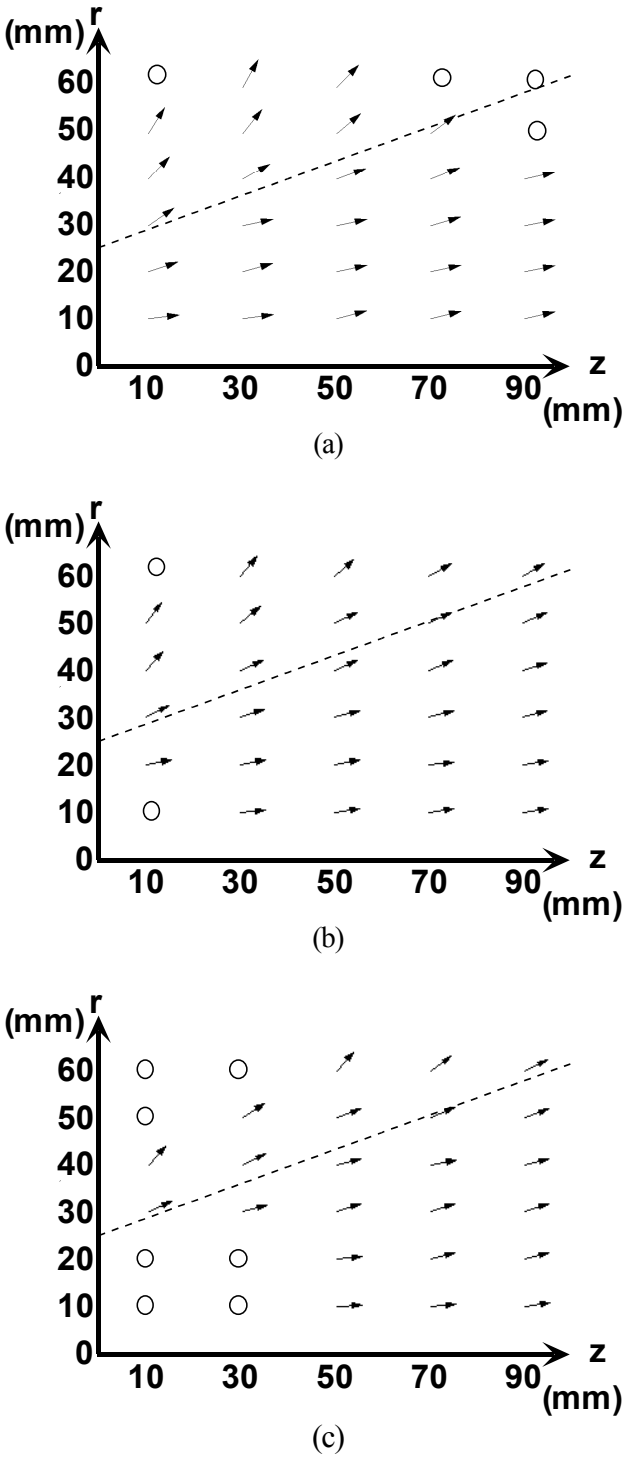

Figure 10 Plasma flow patterns in exhaust plumes from nozzle exit to axial position of 90 mm with Ar and H_2. The dashed lines represent the extrapolation line of the divergent nozzle. (a) Ar, 1.37 g/s, 4 kA; (b) Ar, 1.37 g/s, 8 kA; (c) H_2, 0.40 g/s, 8 kA.

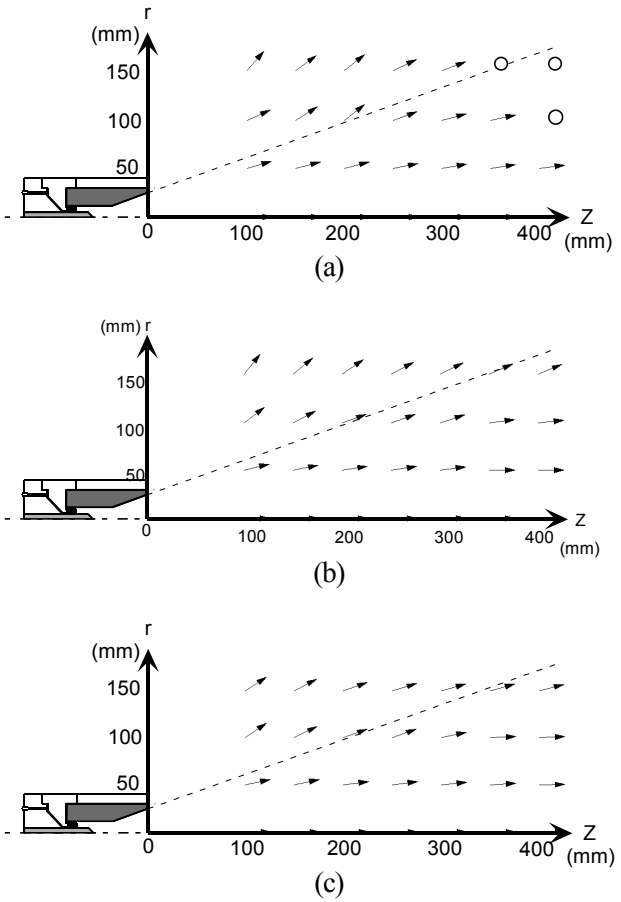

Figure 11 Plasma flow patterns in exhaust plumes from axial position of 100 mm to 400 mm with Ar and H_2. The dashed lines represent the extrapolation line of the divergent nozzle. (a) Ar, 1.37 g/s, 4 kA; (b) Ar, 1.37 g/s, 8 kA; (c) H_2, 0.40 g/s, 8 kA.

converted downstream into axial kinetic energy, and the axial plasma acceleration decreases both the physical properties.

As shown in Figs.12(a) and 12(b), the electron temperature for Ar at 4 kA gradually decreases downstream with radial positions of 0 and 50 mm. However, the temperature at 8 kA extremely decreases although, at enough downstream positions of 300-400 mm, it hardly changes and about 7000 K. Also, the Ar plasma densities at 4 and 8 kA, as shown in Figs.13(a) and 13(b), intensively decrease axially within a radial position of 50 mm although they are almost kept $5x10^{18}$ m^{-3} at 4 kA and $2.5x10^{19}$ m^{-3} at 8 kA at axial positions of 300-400 mm. For H_2, both the distributions of electron temperature and plasma density, as shown in Figs.12(c) and 13(c), are almost flat from an axial position of 100 mm to about 300 mm within a radial position of 50 mm, and they gradually decrease to about 22500 K to about $4.5x10^{19}$ m^{-3}, respectively, downstream from 300 mm. At radial positions of 100 and 150 mm, both the properties intensively

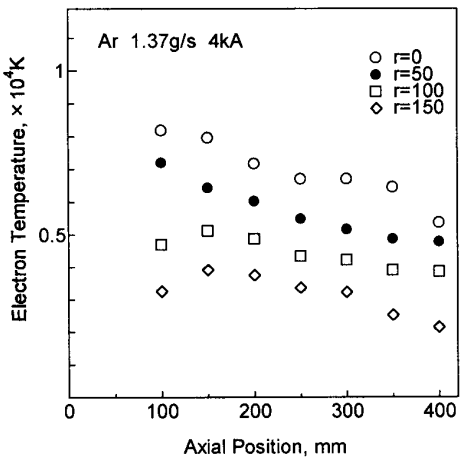

(a)

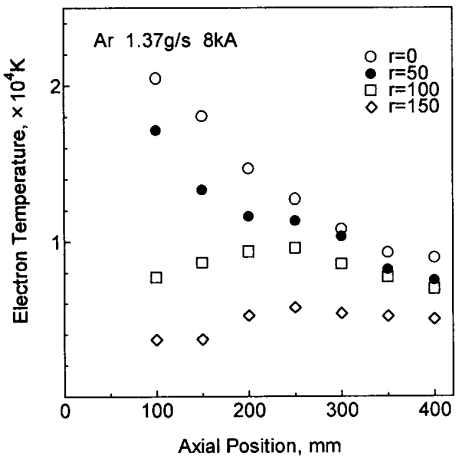

(b)

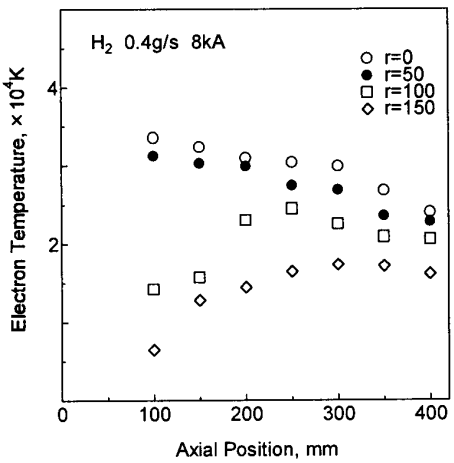

(c)

Figure 12 Axial distributions of electron temperature in exhaust plumes with Ar and H_2 by double probe measurement. (a) Ar, 1.37 g/s, 4 kA; (b) Ar, 1.37 g/s, 8 kA; (c) H_2, 0.40 g/s, 8 kA.

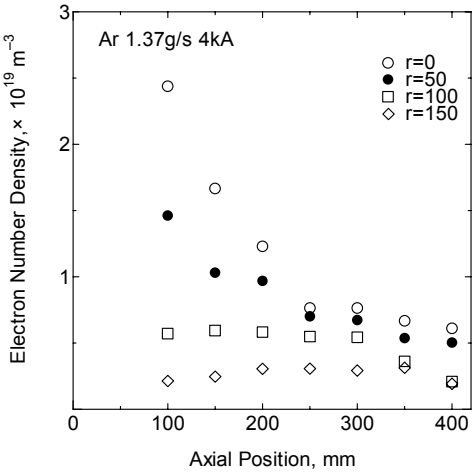

(a)

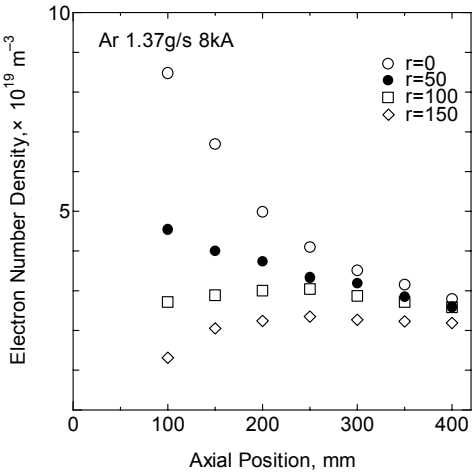

(b)

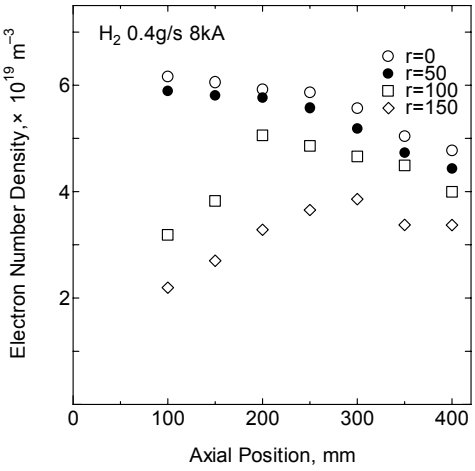

(c)

Figure 13 Axial distributions of plasma number density in exhaust plumes with Ar and H_2 by double probe measurement. (a) Ar, 1.37 g/s, 4 kA; (b) Ar, 1.37 g/s, 8 kA; (c) H_2, 0.40 g/s, 8 kA.

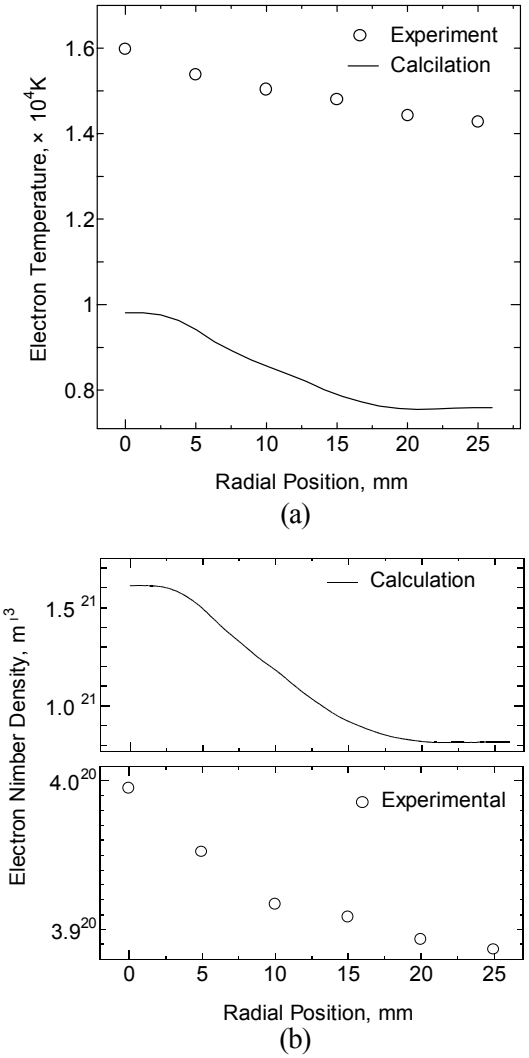

Figure 14 Calculated and experimental results of radial distributions of electron temperature and plasma number density on arcjet nozzle exit with Ar and 4 kA. (a) electron temperature; (b) plasma number density.

increase axially from 100 to 200-250 mm and then gradually decrease downstream. Therefore, a distinct boundary between the inner and outer flows is created with H_2. As shown in Figs.12(b), 12(c), 13(b) and 13(c), the electron temperature for H_2 is relatively large compared with that for Ar, and the plasma density for H_2 is also larger at enough downstream positions of 300-400 mm than that for Ar. This is expected because of the intensive pinch effect for H_2.

Comparison with Calculated Results

Figure 14 shows the calculated and experimental results of the radial distributions of electron temperature and plasma number density on the arcjet nozzle exit with Ar and 4 kA. The calculated electron temperature gradually decreases radially outward as well as the measured one although it is

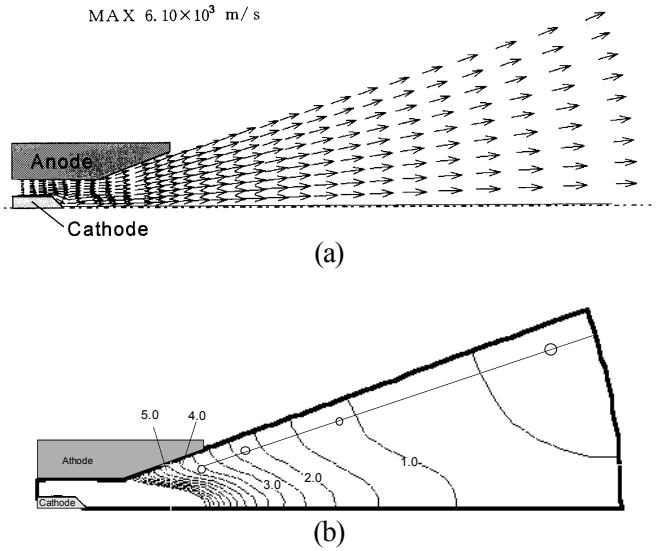

Figure 15 Calculated patterns of plasma velocity vector and ion flux with Ar and at 4 kA. The dashed line represent an equi-ion-flux-line of 90 % on the total flux. (a) plasma velocity vector; (b) ion flux.

lower than the measured one at a constant radial position. On the other hand, the calculated plasma density also decreases radially outward although it is higher than the measured one. Although the calculated electron temperature and plasma density characteristics qualitatively agree with the measured ones and quantitatively for some part of all calculation results, lots of improvement of the calculation model and method are needed.

Plasma Velocity Vector and Ion Flux

Figure 15 shows the calculated patterns of plasma velocity vector and ion flux with Ar at 4 kA. In Fig.15(b), an equi-ion-flux-line of 90 % on the total flux is represented with the dashed line. The plasma is intensively accelerated in the discharge chamber by a strong Lorentz force, and then it smoothly flows downstream through the nozzle outside the discharge chamber. The maximal velocity of 6100 m/s is achieved at the nozzle exit on the central axis in the cathode jet. The number density of Ar^+ was very high near the cathode tip, i.e., in the cathode jet. As a result, a high-temperature, high-number-density and highly-ionized plasma was generated near the cathode tip. As shown in Fig.15(b), the ion flux gradually decreases downstream by radial expansion, and at a constant axial position it is very high near the central axis. Because the large fraction of 90 % of ion flux exists within the dashed line nearly along the nozzle extrapolation line, nozzle angle may influence contamination of spacecraft although a core flow, i.e., the cathode jet, with a large ion flux exists on the central axis.

Conclusions

The quasi-steady MPD thruster MY-III was operated to study the exhaust plume characteristics. Both emission spectroscopic and rotatable double probe measurements were made to evaluate electron temperatures, plasma number densities and plasma flow directions in the downstream plume region. Flowfield calculation was also carried out to understand plasma flow features and acceleration processes in detail. The plasma was slightly expanded radially outward downstream within the extrapolation line of the divergent nozzle regardless of discharge current and gas species although it was intensively expanded outside the line. Therefore, the plasma flow was divided into inner and outer flows with the nozzle extrapolation line. Both the electron temperature and the plasma number density decreased radially outward at a constant axial position. In the outer flow, radial expansion intensively occurred, and both the properties were seen to decrease axially. In the inner flow, a large amount of thermal energy was expected to be smoothly converted downstream into axial kinetic energy, and the axial plasma acceleration decreased the electron temperature and the plasma density. The angle of radial expansion decreased with discharge current because of increasing axial velocity. The angle for H_2 was relatively small compared with cases for Ar because of an intensive thermal pinch effect for H_2. The calculated physical properties qualitatively agreed with the measured ones even with the simple calculation model of one-fluid, one-temperature and no wall losses etc. The calculated ion flux gradually decreased downstream by radial expansion. Because a large fraction of 90 % of ion flux existed within a radius nearly along the nozzle extrapolation line, nozzle angle may influence contamination of spacecraft although a core flow, i.e., the cathode jet, with a large ion flux existed on the central axis.

References

[1] Uematsu, K., and Kuriki, K.," Effect of Electrode Configuration on MPD Arcjet Performance," IEPC-84-11, 1984.

[2] Tahara, H., Kagaya, Y., and Yoshikawa, T.," Effects of Applied Magnetic Fields on Performance of Quasisteady Magnetoplasmadynamic Arcjet," *J. Propulsion and Power*, Vol.11, 1995, pp.337-342.

[3] Mitsuo, K., Tahara, H., Okutani, H., Kagaya, Y., and Yoshikawa, T.," Experimental and Analytical Study of Quasi-Steady MPD Channel Flow," IEPC-97-111, 1997.

[4] Tahara, H., Yamasaki, N., Mitsuo, K., Kagaya, Y., and Yoshikawa, T.," Plasma Features near Quasisteady Magnetoplasmadynamic Arcjet Cathodes," IEPC-97-118, 1997.

[5] Funaki, I., Toki, K., and Kuriki, K.," Numerical Analysis of a Two-Dimensional Magnetoplasmadynamic Arcjet," *J. Propulsion and Power*, Vol.6, 1997, pp.789-795.

[6] Yee, H.C.," A Class of High-Resolution Explicit and Implicit Shock-Capturing Method," NASA TM101088, 1989.